Source of Seasonality and Scale Dependence of Predictability in a Coupled Ocean–Atmosphere Model

B. N. GOSWAMI, K. RAJENDRAN, AND D. SENGUPTA

Centre for Atmospheric Sciences, Indian Institute of Science, Bangalore, India

(Manuscript received 9 June 1995, in final form 3 January 1996)

ABSTRACT

The seasonality of predictability of ENSO (related to the so-called spring predictability barrier) is investigated using the Cane–Zebiak coupled model. Observed winds are used to force the ocean component of the model to generate analyzed initial conditions. It is shown that decrease of predictability during Northern Hemispheric spring is due to fast error growth (with a doubling time of small errors of about seven months) being associated with many, but not all, spring analyzed initial conditions. With winter analyzed initial conditions, errors always grow more slowly (with a doubling time of about 15 months). The fast growth rate of errors seen in the dominant empirical orthogonal function (EOF) in spring is present in all smaller scales of motion (higher EOFs) in all seasons. The coupled model allows initial errors in smaller scales to quickly cascade to the dominant scale in spring of certain years, while it does not allow this in winter. Further, if the initial conditions are generated from a long coupled run (coupled initial conditions as opposed to analyzed initial conditions), then errors in the dominant mode grow slowly both in spring and winter. These results establish that the origin of the seasonality of predictability lies in the use of observed winds to create initial conditions. The authors propose that the analyzed initial conditions have an ''imbalance'' that arises from the fact that the variability of observed winds has a much larger small-scale high-frequency component than model winds. Such imbalances in the spring initial conditions in certain years quickly affect the evolution of the dominant mode, leading to loss of predictability. Even though such imbalances may be present in the winter initial conditions, they take a much longer time to influence the dominant mode, thus accounting for the greater predictability in winter.

1. Introduction

The physical basis for prediction of the mean state of the atmosphere one season or more in advance is well established (Charney and Shukla 1981; Shukla 1981). The premise is that low-frequency changes in the atmosphere (mainly in the Tropics) are governed primarily by slowly varying conditions at the lower boundary such as the sea surface temperature (SST). Many modeling studies (e.g., Lau 1985; Shukla and Fennessy 1988; Shukla and Wallace 1983) and statistical forecasting efforts (Barnett 1981a,b; Barnett and Preisendorfer 1987; Harnack et al. 1986) support this view. In contrast, the subject of predictability of the coupled ocean–atmosphere system is still in its infancy. This is partly because the concept of slowly varying boundary conditions is not relevant to the coupled system. The boundary condition for either component (ocean or atmosphere) is an internal variable for the other (e.g., wind stress or SST). As a result, any long-range predictability in the coupled system must arise from its internal dynamics. By ''internal dynamics'' we mean any process or processes (such as nonlinear interactions or feedbacks) leading to low-frequency oscillations of the coupled system. The dynamics of the coupled system spans a wide spectrum of time and space scales of motion ranging from atmospheric synoptic disturbances, through the annual cycle and biennial oscillation to the quasi-four-year El Niño–Southern Oscillation (ENSO) signal. The fact that the tropical ocean–atmosphere system exhibits a large amplitude ENSO oscillation on the interannual timescale indicates a certain potential for long-range predictability. Extensive studies have been conducted to understand the physical mechanisms of the observed quasi-four-year period, mostly using coupled models including limited but essential physics (see Neelin et al. 1992 for a review). The potential for long-range predictability of ENSO has been demonstrated by several forecasting models including purely statistical methods, intermediate coupled models, and coupled general circulation models (CGCMs). Past work on ENSO prediction, reviewed by Latif et al. (1994), and more recent efforts (Barnett et al. 1994; Ji et al. 1994; Davey et al. 1994; Wu et al. 1994; Balmaseda et al. 1994) have established the possibility of ENSO prediction 6–12 months in advance. Some dynamical coupled models (Cane et al. 1986, in particular) have somewhat

Corresponding author address: Dr. B. N. Goswami, Centre for Atmospheric Sciences, Indian Institute of Science, Bangalore 560 012 India.
E-mail: goswamy@cas.iisc.ernet.in

larger useful lead times. A prominent feature of most of these models is that the skill of forecast has a strong seasonality, with a sharp decline in skill in boreal spring (Xue et al. 1994; Latif et al. 1994) followed sometimes by a recovery of the skill during the following autumn or winter. This so-called spring predictability barrier has been a major concern in attempts to extend the lead time of successful forecasts.

While forecast models have demonstrated the feasibility of forecasting ENSO about one year in advance, the fundamental question regarding the limit on predictability of the coupled ocean–atmosphere system has not been settled. Any further improvement of the present prediction skill of these models will depend on a better understanding of the factors responsible for the limit on predictability, which is determined by the growth of small errors. Goswami and Shukla (1991, hereafter GS) made the first detailed calculation of the growth of small errors in the Cane–Zebiak model (Zebiak and Cane 1987, hereafter CZ model). They showed that growth of small errors in the coupled model is governed by two processes having two different timescales. The fast process has error doubling time of about 5 months (*e*-folding time of about 6.5 months) and the slow process has error doubling time of about 15 months (*e*-folding time of about 21 months). Goswami and Shukla proposed that these two processes may be related to two distinct unstable normal modes of the coupled system. Following a different procedure but using the same model, Blumenthal (1991) also arrived at these two timescales. However, he proposed that the fast error growth arises because the coupled model is non-self-adjoint. If a system is not self-adjoint, there is a possibility of transient growth in a mode that does not coincide with a growing normal mode of the classical stability analysis. This mode is one of the singular vectors of the evolution operator, whose growth rates are given by the singular values (Molteni and Palmer 1993). The growth rate of one (or more) of these transient modes could be larger than that of the fastest growing normal mode. Therefore, if the system is non-self-adjoint, there is a possibility that such transient modes may be relevant to the fast growth of errors. Regardless of whether the fast growing entity in the CZ model is a normal mode or a singular vector, however, it is clear that the predictability of the coupled system is limited by the process or processes responsible for the fastest growth of errors. It is hoped that identification of the origin of the fast error growth will lead to development of methods [similar to initialization in numerical weather prediction (NWP)] to suppress it, and thereby to extend the lead time of useful long-range predictions.

The objective of the present study is to isolate the origin of the fast error growth. Experience with forecast models, which show decrease in forecast skill in spring and enhanced skill in winter, lead us to believe that the fast growth of errors may be linked with the spring predictability barrier. Therefore, we conduct a careful study of the dependence of the error growth on initial conditions. This issue was not dealt with in any detail in GS. Second, a question that has not been addressed in the context of coupled models at all is how errors in different scales of motion grow. Its relevance to the origin of the fast error growth is that the latter may be associated with the smaller scales of motion. The third, related, question is how initial errors in one scale of motion affect the other scales of motion. While these questions have been studied in detail for the predictability of the atmosphere, we have made the first attempt to address them in the context of a coupled ocean–atmosphere model. In addition to being of fundamental importance for understanding the nature of error growth in the coupled system, the answer to these questions has practical relevance. For example, a knowledge of how errors grow in different scales of motion and how errors in one scale affect other scales might indicate what kind of error in the initial condition affects the prediction most severely, and hence cannot be tolerated. On the other hand, errors in the initial condition that do not significantly affect the dominant (ENSO) mode might well be tolerable. As of now, very few observations go into preparing the initial condition for coupled models. We hope that the questions studied here will help to define the optimum set of observations necessary to generate ''good'' initial conditions.

The paper is organized in the following manner. Section 2 describes the model and the methodology, including the design of the experiments. In section 3, we describe a large number of predictability experiments with ''analyzed initial conditions.'' The seasonal dependence of the predictability is examined in detail in this section. The growth of errors in different scales of motion is also examined. In section 4 we discuss predictability experiments with ''coupled initial conditions.'' This section demonstrates that the slow growth of errors is intrinsic to the coupled model, while the fast growth with spring analyzed initial condition must arise due to some high-frequency component introduced through the ''analysis.'' Section 5 summarizes the results and makes some concluding remarks.

2. The model and methodology

a. The model

The model used in this study is the standard version of the Cane–Zebiak model that has been used in a large number of studies related to ENSO (Cane et al. 1986; Zebiak and Cane 1987; Goswami and Shukla 1991, 1993; Blumenthal 1991). This is an anomaly coupled model, that is, the governing equations describe oceanic and atmospheric perturbations about the mean climatological state, with monthly climatology prescribed from observation. The model uses a steady-state atmosphere, and as a result does not contain the effect of atmospheric high-frequency variability on the coupled

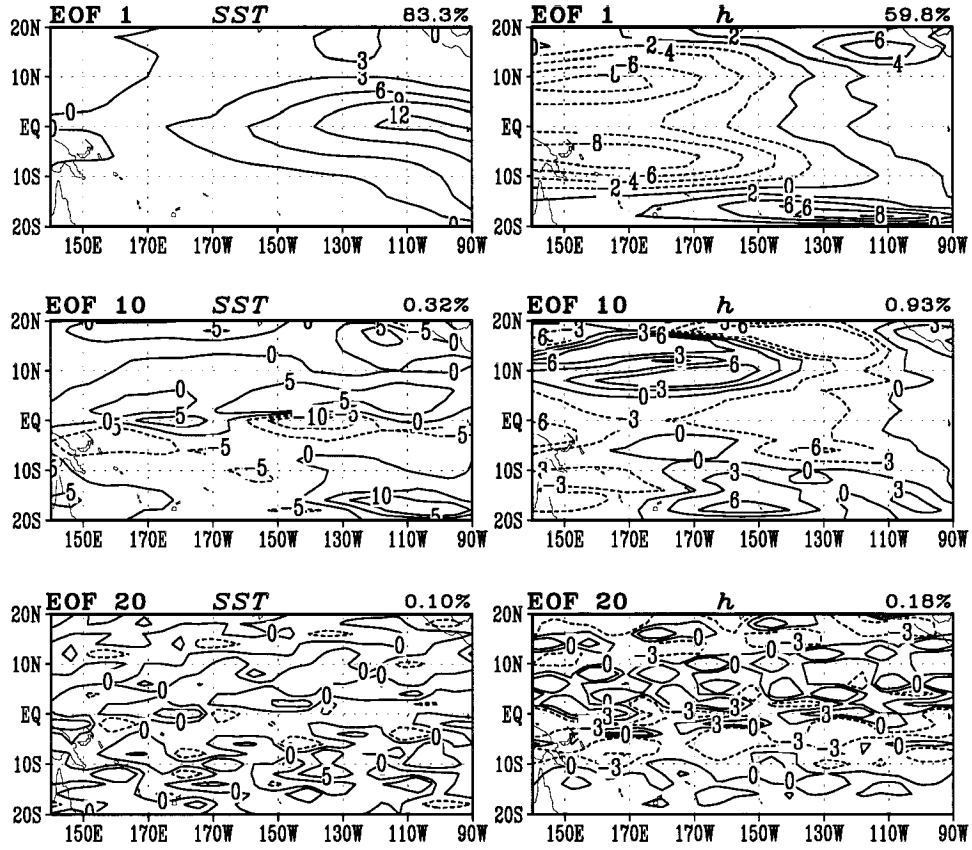

FIG. 1. EOF 1, EOF 10, and EOF 20 of the model sea surface temperature (SST), thermocline height (h), zonal wind (U), and meridional wind (V) anomalies, calculated from monthly values of an 80-yr coupled run. Positive contours are solid lines while negative contours are dashed. The magnitudes of the contours are arbitrary. The percentage of total variance explained by each EOF is also shown.

oscillation. Nonlinearity enters through the thermodynamic energy equation for the ocean. The model is described in many of the studies mentioned above, and we refer the reader to them for details. The strength of this coupled model lies in its ability to simulate much of the characteristic large-scale spatial and temporal structure of ENSO including the recurrence of warm (or cold) phases at irregular intervals with an average period of 3–4 years (Zebiak and Cane 1987). The model prescribes the climatology from observations, and this is equivalent to using a ''flux correction.'' As a result this rather simple model has been more successful in simulating ENSO variability, and in forecasting, than even complex coupled GCMs without flux correction (see Neelin et al. 1992). The weakness of the model lies in the fact that the positive SST anomalies during a mature warm event tend to be too confined meridionally and the core of the positive anomaly does not move sufficiently to the west, compared to reality.

b. Methodology

In GS, predictability experiments were conducted by introducing small perturbations distributed randomly in space. This is equivalent to introducing perturbations in all scales of motion. One of the major objectives of the present study is to examine how errors in different spatial scales of motion evolve and grow. In principle, this may be achieved by representing the model fields in terms of a set of orthogonal functions, Φ_n, each of which has well-defined spatial scales, and then studying the evolution of an initial error having the spatial structure of one of the Φ_n. However, it is not immediately clear how to achieve this in a simple way. ENSO oscillations in the model as well as in nature have a characteristic spatial pattern whose zonal scale is much larger than its meridional scale. It is not possible to represent this pattern by either a small number of Fourier modes or a combination of parabolic cylinder functions and Fourier modes, for example. Therefore, we decided to use the empirical orthogonal functions (EOFs) of the coupled model itself as basis functions to represent the model fields. For this purpose, we carried out EOF analyses of different fields from a long coupled run of the CZ model. The first, tenth, and twentieth EOFs of zonal (U) and meridional (V) winds, sea surface temperature (SST), and thermocline height (h) anomalies are shown in Fig. 1. The dominant mode of variability associated

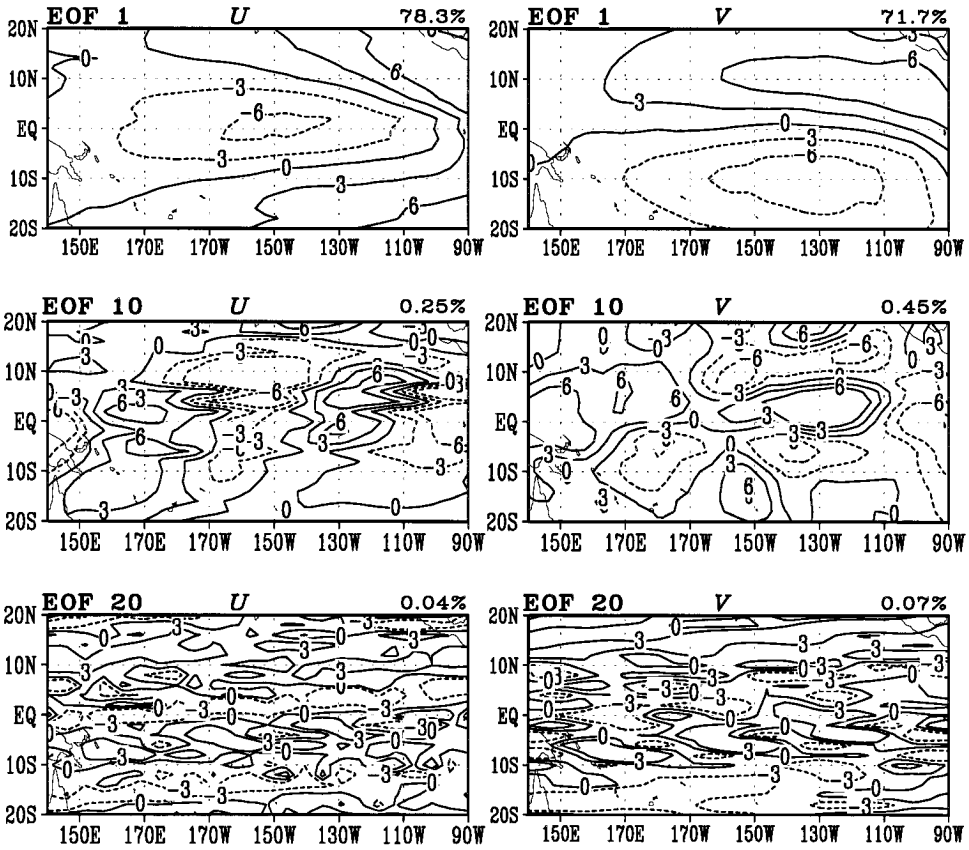

FIG. 1. (*Continued*)

with the ENSO—that is, the first EOF—of any of these fields explains a large fraction of the total variance of that field. EOF 1 explains about 60% of the variance of the *h* field and about 80% of the SST variance. This is consistent with findings in other studies (e.g., Xue et al. 1994; Zebiak and Cane 1991). It is noteworthy that the first four EOFs of the model SST anomalies explain 93.2% of the total variance, whereas the first four EOFs of the observed SST account for 68% of the total variance (Zebiak and Cane 1991). This reflects the partial absence of non-ENSO signal in the model fields, and may be related to the fact that the coupled model has a steady-state atmosphere that does not generate high-frequency atmospheric variability. The full set of EOFs, once calculated from the long coupled run, is called the standard set and is saved for future use in the predictability studies. We recognize that there is no one-to-one correspondence between EOF number (or index) and spatial scale, that is, the *n*th EOF is not necessarily of larger spatial scale than the $(n + 1)$th EOF for all *n*. But EOF 1 is certainly large scale, with basin-scale structure, whereas a high index EOF such as EOF 10 is small scale. We refer to an initial error (see subsection *e*) having the spatial structure of EOF 1 as an error in the large scales of motion and an error with the structure of a high index EOF as being an error in the small scales.

c. Initial conditions

As adequate data for the coupled system variables such as ocean currents and thermocline depth are not available, the initial conditions for the predictability experiments are derived from an initial condition run as described in Cane et al. (1986). In this run, the data (i.e., the values of all fields) at the initial time t_{o_a} is simulated by forcing the ocean component of the coupled model with the wind stress specified from observations for each month starting from January 1964. We have used the Florida State University (FSU) surface wind stress analysis for the period covering January 1964–May 1988 (Goldenberg and O'Brien 1981) to force the ocean component of the coupled model. The calculated anomalies of all model fields including surface winds (as a response to simulated SST) at time t_{o_a} are then saved and used as initial conditions for the predictability experiments. These initial conditions are referred to as the analyzed initial conditions, as they involve the surface wind observations that are assimilated using the model.

Predictability experiments are also carried out with another class of initial conditions, which are referred to as coupled initial conditions. To generate the latter, a coupled model run is started from a chosen analyzed

initial condition at time t_{o_a}. For $t > t_{o_a}$, the coupled model is allowed to generate its own atmospheric and oceanic fields, and the model is integrated up to a time $t = t_{o_c}$. The various oceanic and atmospheric fields at the instant t_{o_c} constitute the coupled initial conditions.

d. Control experiment

A control experiment is a forecast using the coupled model, starting with some initial condition at time t_{o_a}. In the control run, the coupled model produces evolution of both oceanic and atmospheric fields internally for time $t > t_{o_a}$. Generally, control experiments are conducted for a duration of 15 years. The zonal component of surface wind produced by the control run is projected into the set of EOFs of the U field once every month during an experiment. The computed amplitudes of the U field in the different EOFs are saved. This procedure is employed on any field such as SST or h in which we intend to follow the growth of errors. For example, the zonal wind field $U_{\text{Atm}_{\text{Cont.}}}$ in the control experiment is of the form

$$U_{\text{Atm}_{\text{Cont.}}}(x, y, t) = \sum_{n=1}^{N} A_{n_{\text{Cont.}}}(t)\Phi_n(x, y), \qquad (1)$$

where Φ_n is the nth EOF and $A_{n_{\text{Cont.}}}(t)$ is the amplitude (principal component, PC) corresponding to Φ_n; $\{\Phi_n\}$ is the standard set of EOFs that describes the natural variability of the coupled system; and N is the number of model grid points. Since the EOFs are orthogonal, the amplitude corresponding to the nth EOF is

$$A_{n_{\text{Cont.}}} = \Phi_n^T U_{\text{Atm}_{\text{Cont.}}}. \qquad (2)$$

Broadly speaking (see above), EOFs of different indices are associated with different horizontal scales of motion. This property enables us to introduce perturbations selectively to study the growth of errors in the large or small spatial scales and to examine how errors in one scale affect other scales.

e. Perturbation experiments

A perturbation experiment comprises an ensemble of forecast experiments using the coupled model. Each forecast experiment is identical to the control experiment except that a small random perturbation is introduced at the initial time on a selected amplitude A_n. The initial error field corresponding to this perturbation therefore has the spatial structure $\Phi_n(x, y)$. Since the wind stress is an important source of error in the coupled model, the U field was chosen for introducing initial errors. Similarly, to introduce initial error in the ocean component, we chose the thermocline depth field. A number of 15-yr forecast runs, each with a random perturbation to the first amplitude A_1, were conducted. The 15-yr duration is based on our experience that shorter runs often do not permit small initial perturbations to grow to saturation. In these runs, an error is introduced at the initial time t_o in the U field (or the h field) alone. For example, if the initial U field in the control run is

$$U_{\text{Atm}_{\text{Cont.}}}(t_o) = \sum_{n=1}^{N} A_{n_{\text{Cont.}}}(t_o)\Phi_n,$$

then the initial U in a perturbation run is

$$U_{\text{Atm}_{\text{Pert.}}}(t_o) = \{A_{1_{\text{Cont.}}}(t_o) + \delta R\}\Phi_1 + \sum_{n=2}^{N} A_{n_{\text{Cont.}}}(t_o)\Phi_n, \quad (3)$$

where δ is the (fixed) magnitude of the perturbation and R is a random number drawn from a Gaussian set with zero mean and unit variance. The initial perturbation in the amplitude of Φ_1 in the U field leads to differences between the perturbation and control runs in all model fields as time progresses. In general, at any time $t > t_o$, the amplitudes $A_{n_{\text{Pert.}}}(t)$ for any variable in the perturbation run are different from those in the control run, $A_{n_{\text{Cont.}}}(t)$. For example, if

$$U_{\text{Atm}_{\text{Pert.}}}(x, y, t) = \sum_{n=1}^{N} A_{n_{\text{Pert.}}}(t)\Phi_n(x, y)$$

is the U field in the perturbation run, then, in general, $A_{n_{\text{Pert.}}}(t) \neq A_{n_{\text{Cont.}}}(t)$. Perturbation experiments with known initial perturbations on A_n, $n > 1$, have also been carried out.

This method is clearly distinct from the classical studies on predictability such as GS. There, an initial condition run was made by forcing the ocean model with observed surface wind stresses. A series of identical twin experiments with the coupled model was conducted by introducing small initial perturbations randomly distributed in space in each of 181 different initial conditions. Then, the mean error growth was computed by averaging over these 181 experiments. Clearly, the classical studies are not designed to examine the dependence of error growth on initial condition or spatial scale.

f. Error growth analysis

We use the root-mean-square differences (rmse's) of the amplitudes A_n in the control and corresponding perturbation experiments as a measure of error evolution. For an ensemble of perturbation runs containing M samples, the rmse for the kth amplitude at a particular time is

$$\text{rmse}(t) = \left(\frac{1}{M}\sum_{i=1}^{M}\{A_{k_{\text{Cont.}}}(t) - [A_{k_{\text{Pert.}}}(t)]\}^2\right)^{1/2}. \quad (4)$$

To estimate the rate of growth of forecast errors, the classic method used by Lorenz (1982) with modifications suggested by Dalcher and Kalnay (1987) is adopted. The growth of the root-mean-square error E between two forecasts with the same model is assumed to obey the quadratic differential equation

$$\frac{dE}{dt} = \alpha E\left(1 - \frac{E}{E_\infty}\right). \quad (5)$$

Here, α is the rate of growth and E_∞ is the asymptotic value of E. This equation takes into account the exponential growth of a small error with a growth rate α, as well as the eventual saturation of the error at a level E_∞ due to quadratic nonlinearities.

According to Eq. (5), the error evolves as

$$E(t) = E_\infty - \frac{E_\infty}{1 + \left(\frac{E_0}{E_\infty - E_0}\right)e^{\alpha t}}, \quad (6)$$

where E_0 is the initial value of the error.

We need a slight generalization when two processes coexist that lead to two timescales of error growth. We write the total error as

$$E(t) = E_1(t) + E_2(t), \quad (7)$$

where E_1 or E_2 individually is governed by an equation having the form of Eq. (5); α_1 and α_2 represent the two growth rates, and E_{1_∞} and E_{2_∞} the two saturation levels for E_1 and E_2. The error eventually saturates at the level E_∞, which is the sum of the two saturation levels; that is,

$$E_\infty = E_{1_\infty} + E_{2_\infty}. \quad (8)$$

There is no rigorous theoretical basis for fitting the error growth curves with two timescales. This is primarily based on strong empirical evidence and the following arguments. The errors in different scales in systems possessing many scales of motion tend to grow at different rates and saturate at different levels (Lorenz 1969). The growth of errors in a given variable, in principle, has contributions from all these scales. If the growth rates and saturation levels of the errors associated with different scales are not sufficiently well separated, the error for a given variable would show a smooth averaged growth. If, however, the major contribution to the error growth comes from two scales whose growth rates and saturation levels are distinctly different, we expect to see two levels of saturation (or two plateaus) in the error growth curve. In GS it was noted that the averaged error growth in the CZ model has two slopes and two levels of saturation. This led to the proposal that the growth of error in the coupled system is governed by two timescales. In the present study it is shown that the two timescales proposed by GS actually come from different initial conditions, in each of which individually the error in the dominant mode grows with one or the other growth rate. In addition, it is found that errors in all smaller scales of motion tend to have two saturation levels. Therefore, we fit these error curves with the generalized model having two timescales of error growth [Eq. (7)].

3. Predictability experiments with analyzed initial conditions

a. Small initial perturbations on the dominant mode

In this section we present results of a series of identical twin experiments with analyzed initial conditions from the period January 1970–December 1987. For each initial condition a 15-yr control coupled run is made. During the control experiment the projected amplitudes $A_n(t)$ for any field (say, U) are saved every month. Then, an ensemble of perturbation runs (normally 10, often more than 100), each of 15 years' duration, is made introducing a random perturbation in one of the amplitudes (say, A_1 or A_{10}) at the initial time in each case. The magnitude of the perturbation is a fixed percentage of the standard deviation of the corresponding amplitude. We have examined the evolution of both small and large initial errors. In the small error experiments, the initial error in A_1 is equal to 1% of its standard deviation (SD), whereas initial error in A_{10} is 10% of the SD of A_{10}. These values are chosen because high-index EOFs explain a much smaller fraction of the variance of any physical field. The large error experiments have initial error magnitudes of up to 20% of the SD of A_1. The standard deviation of each amplitude represents the upper bound or the level of saturation of errors in that amplitude.

In the first set of experiments, initial errors were introduced in the dominant amplitude A_1 for the U field. Figure 2 shows the time evolution of A_1 from the control and fifty perturbation runs, and of the rmse [Eq. (4)], for the different analyzed initial conditions, one corresponding to Northern Hemisphere spring (April) and the other corresponding to winter (December). All perturbation trajectories are close to the control for some time and then move away from it (and from each other). It is remarkable that the rmse curves show large fluctuations, which persist even if the ensemble size of the perturbation runs is increased to 200 (not shown). Inspection of several cases shows that mean peak-to-peak separation is roughly two years (Fig. 2a); in some cases (Fig. 2b), the fluctuations are modulated by an oscillation of about 4-yr period.

It also appears that with December initial conditions the perturbation trajectories are close to the control for a longer period than in the May case (Figs. 2a,c). Further, the root-mean-square (rms) difference seems to grow slower and to take longer to reach saturation in the winter case than in the spring case (Figs. 2b,d). The saturation level is approximately equal to the SD of A_1 for the U field, which is about 18.

To decide how the winter and spring error growths differ from each other, we need a quantitative estimate of the growth rate. This is made difficult by the presence of the large fluctuations in the rmse curves. If we club together several winter cases or several spring cases from different years, the amplitude of the fluctuations are found to reduce substantially. Although the rmse

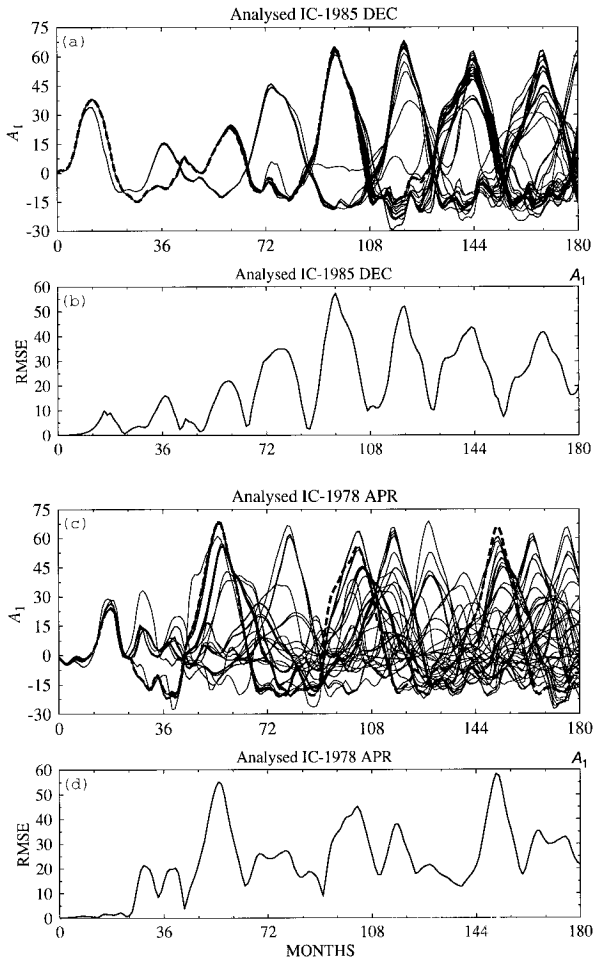

FIG. 2. The time evolution of the dominant amplitude (A_1) of the zonal wind field (U) in a control (thick dashed) run and 50 perturbation (thin lines) runs for a winter [(a) 1985 December] and a spring [(c) 1978 April] analyzed initial condition. The evolution of rmse in A_1 for the two initial conditions is shown in (b) and (d), respectively. The initial perturbation is applied to A_1 of U and its magnitude is equal to 1% of the standard deviation of A_1.

curve for each April (or December) has similar large amplitude oscillations, the curves for different years are phase shifted relative to each other, resulting in the reduction of the fluctuations in the composite. The phase shift of the rmse curves is due to the phase shift of the control runs corresponding to different Aprils (or Decembers). Figure 3 shows the rms errors from a composite of 18 winter cases with December initial conditions from 1970 to 1987. For each analyzed initial condition, a control and 10 perturbation runs were made; the rms error evolutions for the different initial conditions were averaged over the 18 cases to form the composite. The initial error in A_1 propagates to all other amplitudes A_n as the integration proceeds. The dotted curves represent the best fit to the rmse evolution using either Eq. (6) or Eq. (7). The rmse for A_1 clearly has only one saturation level, whereas those for higher amplitudes have two saturation levels. A good fit cannot be obtained for any A_n, $n > 1$ using a single growth rate and saturation level.

It is easy to show that for small initial error ($E_o/E_\infty \ll 1$) the error as given by Eq. (5) grows exponentially for small times ($\alpha t \ll 1$). The fit to the rmse curve for A_1 allows the estimation of the growth rate α_1; for the December initial conditions α is 0.05 and this corresponds to a doubling time of small errors of about 15 months. All higher amplitudes A_n have two growth rates, the smaller of which is about 0.1 for all n. The errors behave in exactly the same way for January initial conditions.

Spring initial conditions seem to fall into two classes. In some years the growth of error in A_1 is slow and its behavior is similar to the winter case; in other years, error growth is much faster. The rmse with the first class of spring initial conditions is not shown. We mention only that error in A_1 has one growth rate ($\alpha \approx 0.05$), whereas error in any higher A_n has two growth rates, the lower of which is about 0.1. We therefore call these spring cases winterlike. Of the 18 years examined (1970–87), eight April initial conditions are winterlike. Very few of the May initial conditions exhibit fast growth; in many of the May cases, an initial period of very slow growth seems to be followed by sudden increase of the growth rate.

The rmse curves from the remaining 10 April initial conditions, which exhibit fast error growth in A_1, have been composited (Fig. 4). Once again, error in A_1 has a single growth rate, and higher A_n show two growth rates. The value of α is 0.1, corresponding to a doubling time of about 7 months. The smaller of the two growth rates in the higher amplitudes is again about 0.1. Unlike in the winter cases, there is significant scatter in the growth rate of small errors in A_1 within the different Aprils that have gone into the composite. In some years the growth is relatively slow (though distinctly faster than in winter) and in some years the growth is almost twice as fast.

We find that the essence of the seasonality of error growth is the following. Errors in the dominant mode in all runs with winter initial conditions grow slowly, whereas in about half of all spring cases they grow fast. The fast growth rate in A_1 in spring, with doubling time of about seven months, is present in the higher EOFs in all cases irrespective of initial condition, indicating that it is a characteristic growth rate for the smaller scales of motion. It appears that this fast growth rate invades A_1 in spring in certain years, while it is unable to do so in winter.

Goswami and Shukla (1991) found that error evolution seems to be governed by two growth rates. Their estimates of the rates are not very diffferent (doubling times of 15 and 5 months) from the slow and fast growth rates found here. However, since the rmse was averaged over all initial conditions, the origin of the fast growth was not clear in GS.

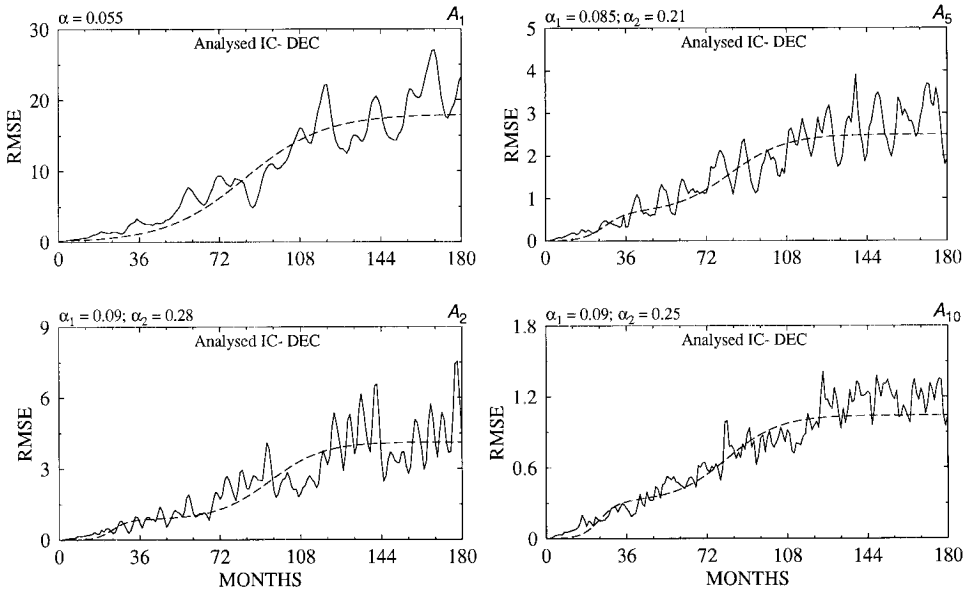

FIG. 3. Evolution of rmse composite for amplitudes A_1, A_2, A_5, and A_{10} of the zonal wind field (U) with winter analyzed initial condition. The composite is made from 18 December analyzed initial conditions from 1970 to 1987. The dashed curves represent empirical fits to the error curve. The initial perturbation is applied to A_1 of U and is equal to 1% of the SD of A_1 (which corresponds to 1.6% of the total variance of the U field). The quantities α, α_1, and α_2 are growth rates.

So far we have discussed growth of errors when initial errors are introduced in an atmospheric field (zonal wind). The growth of errors in the coupled system is expected to be governed by coupled dynamics. Therefore, it should be immaterial whether the initial errors are in an atmospheric field or in an oceanic field. To test this we carried out a series of experiments for a number of initial conditions where a small error was introduced in the dominant mode (A_1) of the thermocline depth field (h). This is equivalent to introducing initial error in the oceanic heat content. The rmse for the prediction of thermocline height anomaly (not shown) evolves in much the same way as the rmse for zonal wind in all cases examined. Our main conclusions regarding the error growth seem to be valid regardless of whether the initial error is in an atmospheric field or in an oceanic field.

As the dominant mode (EOF 1) explains a very large fraction of the total variance of any variable in the model, the error growth in any particular physical field should be dominated by the error growth in its first EOF. To test whether this is the case, we looked at the growth of errors in SST and zonal wind anomalies averaged over the Nino-3 (5°S–5°N; 150°–90°W) and Nino-4 (5°S–5°N; 160°E–150°W) regions in a few cases. Examination of rmse in Nino-3-SST or Nino-3-U, Nino-4-SST or Nino-4-U, shows that evolution of errors in these fields is nearly the same as that in the dominant mode. Clearly, the growth of errors in the dominant mode determines the error growth of the model fields. The assertions in this and the previous paragraph are based on only a few initial conditions, and should be considered preliminary.

b. Initial perturbation on high EOFs (small scale)

In this section, we address the following important issue. How do errors initially introduced in small spatial scales influence the growth of errors in the dominant mode? To answer this question, we introduce an initial error in the tenth EOF, whose magnitude is 10% of the SD of A_{10}. The growth of rmse in the dominant mode (A_1) for winter and spring initial conditions is shown in Fig. 5. Figure 5a is the average over six December initial conditions and Fig. 5b is a composite formed from seven non-winter-like April cases. The first thing to note is that whether the initial error is in the dominant mode (as in Figs. 3 and 4) or in a higher mode (as in Fig. 5), the rate of growth of errors in A_1 remains the same. Errors grow slowly with winter initial conditions and fast with spring initial conditions. The second, and perhaps the more important point to note is the following. The magnitude of the initial error introduced in the tenth EOF is the same for both winter and spring initial conditions, and the level of saturation of errors in A_1 is the same for all initial conditions. Since the rates of growth of errors for spring and winter initial conditions are clearly different, one would expect the time required to reach saturation with winter initial conditions to be longer than that with spring initial conditions (as can be seen in Figs. 3 and 4). If the initial error is in A_{10}, however, we note from Fig. 5 that while the time taken

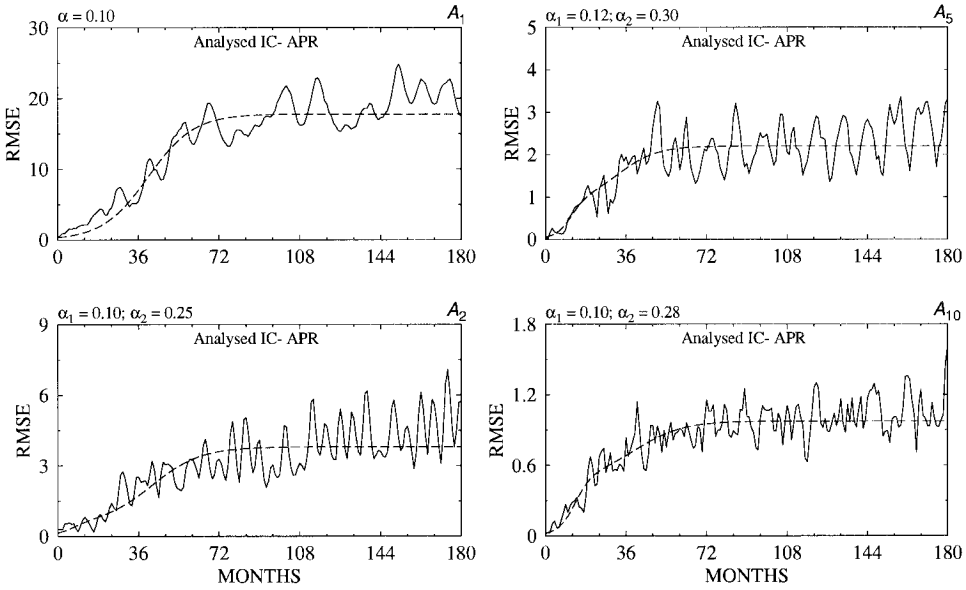

FIG. 4. Same as in Fig. 3 but for spring analyzed initial condition. The composite is made from 10 non-winter-like April analyzed initial conditions.

for error to reach saturation with spring initial conditions is comparable to those in Fig. 4, the corresponding time with winter initial conditions is much larger than those in Fig. 3. With winter initial conditions, error in A_1 does not reach saturation in a 15-yr integration, and therefore we made 30-yr integrations in this case. The implication is that a perturbation of small spatial scale quickly introduces a significant error in the dominant mode in spring but takes much longer to lead to an appreciable error in EOF 1 in winter. In other words, it appears that the dynamics of the coupled system allows errors in small-scale motions in spring to propagate rapidly to the dominant mode, while it discourages upscale propagation of small-scale winter errors.

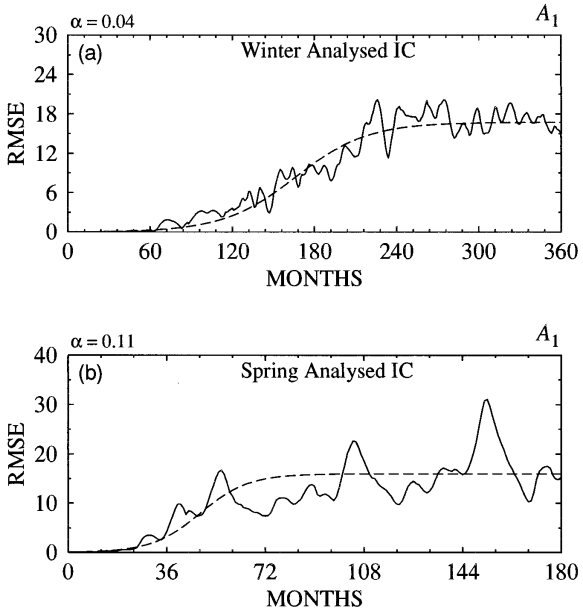

FIG. 5. Evolution of rmse composite (solid curve) with empirical model fit (dashed curve) for the dominant amplitude (A_1) for (a) winter and (b) spring analyzed initial conditions. For each initial condition, an ensemble of 10 perturbation runs were made. The initial perturbation is applied to A_{10} of U and its magnitude is equal to 10% of the SD of A_{10}. The rmse are composited from six winter and seven spring initial conditions.

c. *Large initial perturbation on the dominant mode*

Our interest in the present study is chiefly to examine seasonality and scale dependence in the growth of small initial errors. As pointed out in the introduction, it is the behavior of small errors that determines the theoretical limit on predictability. However, when the CZ model is used for making predictions, the errors in the initial fields are not necessarily small. Further, it is the behavior of the error in the first couple of years that is of greatest interest in prediction-related work. An anonymous reviewer has noted that very small errors grow so slowly in the first year or so, that it might be of interest to examine the growth of more realistic errors.

Accordingly, we discuss the initial evolution of errors in EOF 1 of magnitude equal to 5%, 10%, and 20% of the SD of A_1. Figure 6 shows the rmse evolution in A_1 in the first three years. Errors with December and January initial conditions are composites of all 18 cases examined and those for April are composites of the 10 fast April cases (as in section 3a). The case of small initial error (1% of the SD of A_1) is shown for reference (top panel). There are two important things to note in Fig. 6. First, seasonality is marked for small initial error,

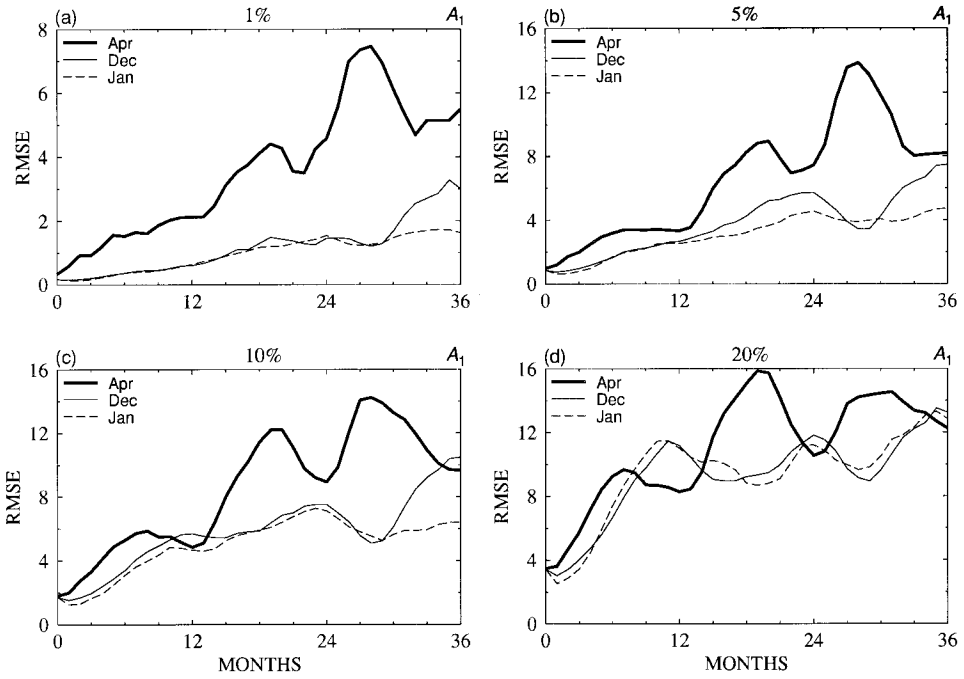

FIG. 6. Evolution of rmse composite in the first 3 years in the dominant amplitude (A_1) with winter (December, January) and spring (April) analyzed initial conditions with initial error in the dominant mode of U. The magnitude of error is equal to (a) 1%, (b) 5%, (c) 10%, and (d) 20% of the SD of A_1. The December and January composites are based on 18 initial conditions each while the April composites are based on 10 non-winter-like April initial conditions.

and is discernible also in the 5% and 10% cases, whereas the 20% case shows no consistent seasonality. Second, the rate of growth of error in the first year increases as the size of the initial error is increased; this is true for both spring and winter initial conditions.

For small and moderate initial error (the 1%, 5%, and 10% cases), the rmse with April initial conditions is always higher than that with winter initial conditions. As the initial error magnitude is increased to 20% of the SD of A_1, however, rmse at 12 months is higher in the winter cases than in the April case, leading to loss of any seasonality. We remind the reader that in all these experiments the initial perturbation has the spatial structure of EOF 1 and is therefore large scale. In an actual forecast, the errors in the initial fields will almost certainly have nonzero projections on higher EOFs as well; that is, they will have a component with smaller spatial scales as well.

4. Predictability experiments with coupled initial conditions

So far we have discussed the growth of errors in forecasts with analyzed initial conditions, which are derived by forcing the ocean component of the coupled model with observed wind stress. Below, we examine the growth of errors in forecasts with initial conditions generated by the coupled model itself.

To generate coupled initial conditions, the coupled model was run for a selected duration, T, starting with the analyzed initial condition at time t_{o_a}. During this run, the model generates its own evolution of atmospheric as well as oceanic variables. The full set of fields at the time $t_{o_c} = t_{o_a} + T$ constitutes the coupled initial condition. The control run, and a set of 10 perturbation runs are made with coupled initial conditions for a duration of 15 years. The methodology for studying the growth of errors in different scales of motion is identical to that described in the case of analyzed initial conditions.

First we show in Fig. 7 the rmse for the dominant mode (A_1) for winter and spring coupled initial conditions. The upper panel is a composite based on six winter coupled initial conditions and the lower panel on six April coupled initial conditions. Each coupled initial condition, at time t_{o_c}, has been generated by starting at t_{o_a} from an analyzed initial condition and running the coupled model for a long time T (at least 20 years). Small perturbations were introduced in the dominant mode of the U field at time t_{o_c} ($= t_{o_a} + T$). The striking feature is that errors in both spring and winter cases tend to grow with the slow growth rate. The fast growth rate seen with spring analyzed initial conditions (section 3a) is conspicuous by its absence in the dominant mode. However, as with the analyzed initial conditions, fast growth is inherent to the higher EOFs (not shown). It therefore follows that the slow timescale is the intrinsic timescale of the coupled model. The lack of seasonality in the growth of errors with coupled initial conditions

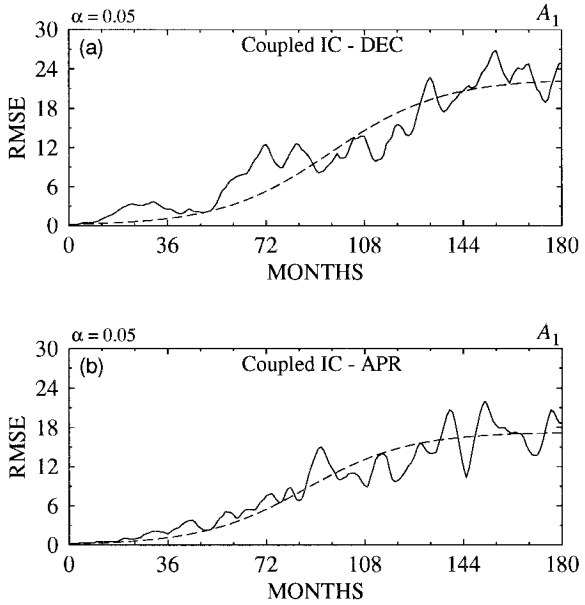

FIG. 7. Evolution of rmse composite with empirical model fit for the dominant amplitude (A_1) with (a) winter (December) and (b) spring (April) coupled initial conditions for large T. Here, T is larger than 20 years in all cases. The initial perturbation is applied to A_1 of U and is equal to 1% of the SD of A_1.

and the presence of clear and marked seasonality with analyzed initial conditions clearly shows that fast growth of errors must be somehow related to the analysis, which uses the observed surface wind history to generate initial conditions.

Having established that the rapid error growth in the model with spring initial conditions is related to the analysis, we ask the following question. For how long does the coupled model retain the memory of the analyzed initial conditions? To answer this question, we conducted another series of identical twin experiments with coupled initial conditions, with t_{o_c} not very far from t_{o_a}, that is, with relatively small values of T. Figure 8 shows composites of rmse in the dominant mode with for four different kinds of coupled initial conditions with T lying between 12 and 20 months in each case. Each of these composites is based on six similar initial conditions. We see that if T is small, the growth of errors is still governed by the model's memory of the analyzed initial condition. In other words, if the coupled model was started with spring analyzed initial condition, the growth of error is fast, no matter whether we initiate the predictions from next winter or spring. Similarly, if the coupled model was initiated with winter analyzed initial conditions, the error grows slowly regardless of whether the coupled initial conditions pertain to spring or winter. We have found from experiments with different coupled initial conditions that the coupled model begins to lose its memory of the analyzed initial conditions after 3–4 years.

5. Summary and conclusions

The predictability of short-term climate fluctuations such as ENSO, involving the coupled ocean–atmosphere system, is primarily governed by internal dynamics. The

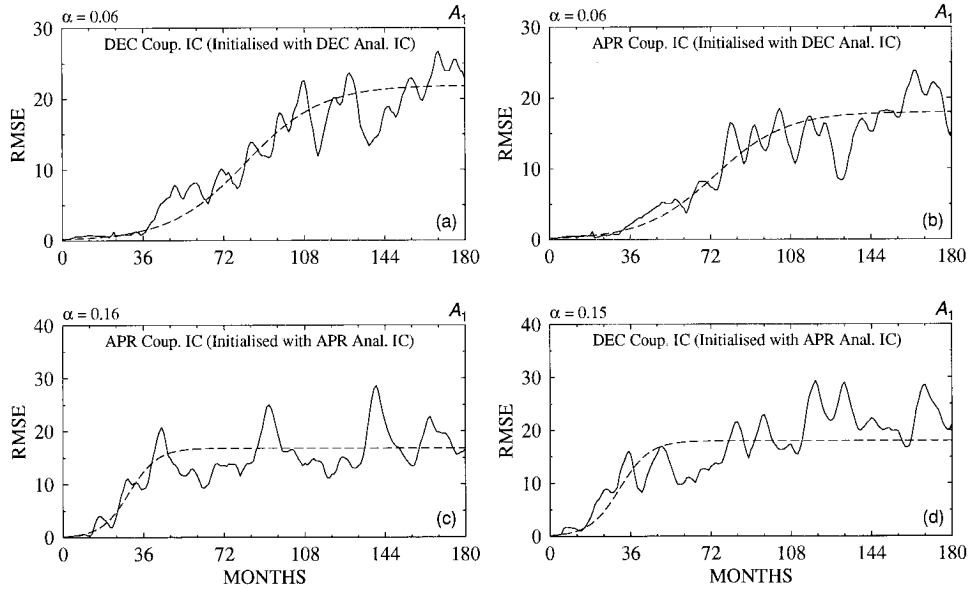

FIG. 8. Evolution of rmse composite with empirical model fit for the dominant amplitude (A_1) for small T with (a) winter (December) and (b) spring (April) coupled initial conditions derived from winter analyzed initial conditions and with (c) spring and (d) winter coupled initial conditions derived from spring analyzed initial conditions. Here, T is smaller than two years in all cases. The initial perturbation is applied to A_1 of U and is equal to 1% of the SD of A_1.

physical basis for any long-range predictability of such a system lies in the existence of one or more low-frequency internal oscillations with significant amplitude. The limit on the predictability, however, is set by growth rates and saturation levels of errors in different scales of motion in the presence of interaction between scales. While these issues have been extensively studied in atmospheric predictability, they have not been examined at all for the coupled ocean–atmosphere system. Recent studies have shown that the growth of errors in the coupled system is governed by at least two timescales (GS; Blumenthal 1991). One of these is fast, with an error doubling time of about 5 months, and the other is slow, with a doubling time of about 15 months. To put these growth rates in perspective, an initial error of 0.25°C in SST would take a year to grow to 1.5°C (approximately the SD of Nino-3 SST anomalies) at the fast rate, and over three years at the slow rate. Present-day forecast models (Latif et al. 1994) have useful prediction skill at lead times of 6–12 months. Some intermediate dynamical models (specially the CZ model) show skill at lead times of 12–18 months. It seems clear that the skill of this class of models is limited by rapid growth of error, at a rate comparable to the fast rate identified in GS. The primary objective of the present study is to investigate the origin of the fast error growth. We do this by examining the seasonal and scale dependence of error growth. Decomposition of model fields in terms of the model's EOFs allows us to introduce errors with a given spatial structure and to study growth of errors in all scales.

We have studied the growth of errors in forecasts started from different seasons. Two classes of initial conditions were used—analyzed initial conditions were generated using past observed winds and the ocean component of the coupled model, whereas a long ($\sim$ 20 yr) run of the coupled model was used to generate coupled initial conditions, in which the atmospheric and oceanic fields are expected to be compatible with each other.

We find that growth of small or moderate error in the analyzed initial condition is always slow in winter forecasts and fast in forecasts started from spring of certain years. If coupled initial conditions are used, there is no such seasonality and errors always grow slowly. Clearly, the slow growth rate of errors (doubling time of about 15 months) is intrinsic to the model, whereas the fast growth rate (doubling time of about 7 months) arises from the use of observed winds in the analysis procedure. There is clearly a mismatch between the physical fields in the analyzed initial condition and the kind of balanced fields that the model demands.

This mismatch leads to the seasonality in error growth. The CZ model was designed specifically to capture the interannual variability of the large spatial scales of motion. Therefore, much of the small-scale component of the fields in the analyzed initial conditions must appear to the model as noise. It is also possible that the analyzed initial condition has error in the large spatial scale. Our experiments show that in either case the consequence is rapid error growth in the dominant mode (EOF 1) with a subset of spring initial conditions.

If we recall that the first four EOFs of the coupled model wind explain 95% of its variance, whereas the corresponding number for the FSU winds is 41% (see GS), it becomes clear that small-scale noise must be present in the analyzed fields both in spring and winter. We have shown (section 3b) that error travels much more quickly from the small scales to the dominant mode with spring initial conditions than with winter initial conditions. This leads to rapid growth of error in the physical fields with spring initial conditions, whereas the growth remains slow in the winter case. If the initial errors are large scale, the growth of error in the dominant mode is fast in the spring case and slow in the winter case (section 3a).

We believe that the ultimate limit on predictability is governed by the slow growth rate of errors in the model. It appears that some improvement of forecast skill may be expected if the amplitude of the small spatial scales in the analyzed fields can be reduced to make the latter more compatible with the model. Of relevance here is the study of Xue et al. (1994), who find that the fastest growing singular vector of the evolution operator in the CZ model has nonzero projection mostly on high-index multivariate EOFs of small spatial scales. Another possibility is an analysis procedure using modified winds, which are more in keeping with the model's demands. Encouraging results have been reported in this direction recently (Chen et al. 1995).

Our results on the source of the fast growth rate of errors in the CZ model may have a broader relevance to the mechanism for the spring predictability barrier common to most prediction models. To put our results into perspective, it is important to point out some limitations of the present study and some unanswered questions. First, our results are based on the CZ model. It is important to establish the robustness of these results using other similar or more complex coupled models. In particular, it would be desirable to study the role of atmospheric high-frequency variability, absent from the present model. Second, the question of cascade of errors from one scale of motion to another has not been examined in any detail in the present study. Further, it is not clear what physical factors determine whether a spring initial condition from a particular year will exhibit slow or fast growth. Many of the May initial conditions show very slow growth of error in the first two or three years if the initial error is small and has large spatial scale. A final question concerns the relative projections of the analyzed fields onto the large-scale and small-scale EOFs of the coupled model. We are taking a close look at the mismatch between the analyzed initial fields and the various physical fields from the coupled model at present.

Acknowledgments. The authors would like to thank

M. A. Cane and S. E. Zebiak for allowing the use of their model. We are also grateful to V. Krishnamurthy for many stimulating discussions and suggestions, and to two anonymous reviewers for their constructive comments. We would also like to thank the Super Computer Education and Research Centre of Indian Institute of Science for the computing facility. This work is supported in part by the Department of Science and Technology, Government of India.

REFERENCES

Balmaseda, M. A., D. L. T. Anderson, and M. K. Davey, 1994: ENSO prediction using a dynamical ocean model coupled to statistical atmospheres. *Tellus,* **46A,** 497–511.

Barnett, T. P., 1981a: Statistical prediction of North American air temperature from Pacific predictors. *Mon. Wea. Rev.,* **109,** 1021–1041.

——, 1981b: Statistical relations between ocean/atmosphere fluctuations in the tropical Pacific. *J. Phys. Oceanogr.,* **11,** 1043–1058.

——, and R. W. Preisendorfer, 1987: Origins and levels of monthly and seasonal forecast skill for United States surface temperatures determined by canonical correlation analysis. *Mon. Wea. Rev.,* **115,** 1825–1850.

——, and Coauthors, 1994: Forecasting global ENSO-related climate anomalies. *Tellus,* **46A,** 381–397.

Blumenthal, M. B., 1991: Predictability of a coupled ocean–atmosphere model. *J. Climate,* **4,** 766–784.

Cane, M. A., S. C. Dolan, and S. E. Zebiak, 1986: Experimental forecasts of El Niño. *Nature,* **321,** 827–832.

Charney, J. G., and J. Shukla, 1981: Predictability of monsoons. *Monsoon Dynamics,* J. Lighthill and R. P. Pearce, Eds., Cambridge University Press, 99–109.

Chen, D., S. E. Zebiak, A. J. Busalacchi, and M. A. Cane, 1995: An improved procedure for El Niño forecasting. *Science,* **269,** 1699–1702.

Dalcher, A., and E. Kalnay, 1987: Error growth and predictability in operational ECMWF forecasts. *Tellus,* **39A,** 474–491.

Davey, M. K., S. Ineson, and M. A. Balmaseda, 1994: Simulation and hindcasts of tropical Pacific Ocean interannual variability. *Tellus,* **46A,** 433–447.

Goldenberg, S. O., and J. J. O'Brien, 1981: Time and space variability of tropical Pacific wind stress. *Mon. Wea. Rev.,* **109,** 1190–1207.

Goswami, B. N., and J. Shukla, 1991: Predictability of the coupled ocean–atmosphere model. *J. Climate,* **4,** 3–22.

——, and ——, 1993: Aperiodic variability in the Cane–Zebiak model: A diagnostic study. *J. Climate,* **6,** 628–638.

Harnack, R., J. Harnack, and J. Lanzante, 1986: Seasonal temperature predictions using jackknife approach with an intraseasonal variability index. *Mon. Wea. Rev.,* **114,** 1950–1954.

Ji, M., A. Kumar, and A. Leetmaa, 1994: An experimental coupled forecast system at the National Meteorological Centre. Some early results. *Tellus,* **46A,** 398–418.

Latif, M., T. P. Barnett, M. A. Cane, M. Flügel, N. E. Graham, H. von Storch, J-S. Xu, and S. E. Zebiak, 1994: A review of ENSO prediction studies. *Climate Dyn.,* **9,** 167–179.

Lau, N. C., 1985: Modeling the seasonal dependence of the atmospheric response to observed El Niños 1962–1976. *Mon. Wea. Rev.,* **113,** 1970–1996.

Lorenz, E. N., 1969: The predictability of a flow which possesses many scales of motion. *Tellus,* **21,** 289–307.

——, 1982: Atmospheric predictability experiments with a large numerical model. *Tellus,* **34,** 505–513.

Molteni, F., and T. N. Palmer, 1993: Predictability and finite-time instability of the northern winter circulation. *Quart. J. Roy. Meteor. Soc.,* **119,** 269–298.

Neelin, J. D., and Coauthors, 1992: Tropical air–sea interaction in general circulation models. *Climate Dyn.,* **7,** 73–104.

Shukla, J., 1981: Dynamical predictability of monthly means. *J. Atmos. Sci.,* **38,** 2547–2572.

——, and J. M. Wallace, 1983: Numerical simulation of the atmospheric response to equatorial Pacific sea surface temperature anomalies. *J. Atmos. Sci.,* **40,** 1613–1630.

——, and M. Fennessy, 1988: Prediction of time-mean atmospheric circulation and rainfall: Influence of Pacific sea surface temperature anomaly. *J. Atmos. Sci.,* **45,** 9–28.

Wu, D.-H., D. L. T. Anderson, and M. K. Davey, 1994: ENSO prediction experiments using a simple ocean–atmosphere model. *Tellus,* **46A,** 465–480.

Xue, Y., M. A. Cane, S. E. Zebiak, and M. B. Blumenthal, 1994: On the prediction of ENSO: A study with a low-order Markov model. *Tellus,* **46A,** 512–528.

Zebiak, S. E., and M. A. Cane, 1987: A model El Niño/Southern Oscillation. *Mon. Wea. Rev.,* **115,** 2262–2278.

——, and ——, 1991: Natural climate variability in a coupled model. *Greenhouse-Gas-Induced Climate Change: A Critical Appraisal of Simulations and Observations,* M. E. Schlesinger, Ed., Elsevier Science Publishers, 457–469.